6924–6934 *Nucleic Acids Research, 2016, Vol. 44, No. 14* *Published online 10 May 2016*
doi: 10.1093/nar/gkw401

Rational engineering of the *Neurospora* VS ribozyme to allow substrate recognition via different kissing-loop interactions

Julie Lacroix-Labonté, Nicolas Girard, Pierre Dagenais and Pascale Legault*

Département de Biochimie et Médecine Moléculaire, Université de Montréal, C.P. 6128, Succursale Centre-Ville, Montréal, QC H3C 3J7, Canada

Received February 19, 2016; Revised April 25, 2016; Accepted April 30, 2016

ABSTRACT

The *Neurospora* VS ribozyme is a catalytic RNA that has the unique ability to specifically recognize and cleave a stem-loop substrate through formation of a highly stable kissing-loop interaction (KLI). In order to explore the engineering potential of the VS ribozyme to cleave alternate substrates, we substituted the wild-type KLI by other known KLIs using an innovative engineering method that combines rational and combinatorial approaches. A bioinformatic search of the protein data bank was initially performed to identify KLIs that are structurally similar to the one found in the VS ribozyme. Next, substrate/ribozyme (S/R) pairs that incorporate these alternative KLIs were kinetically and structurally characterized. Interestingly, several of the resulting S/R pairs allowed substrate cleavage with substantial catalytic efficiency, although with reduced activity compared to the reference S/R pair. Overall, this study describes an innovative approach for RNA engineering and establishes that the KLI of the *trans* VS ribozyme can be adapted to cleave other folded RNA substrates.

INTRODUCTION

The *Neurospora* VS ribozyme belongs to the family of natural nucleolytic ribozymes, which are <200 nt in size and include the hairpin, HDV, hammerhead, *glmS*, twister, twister sister, pistol and hatchet ribozymes (1–5). Like many other ribozymes, the VS ribozyme provides a good model system for fundamental studies of RNA structure and function, which are of value for understanding more complex RNA-mediated processes (6). So far, a large body of *in vitro* work has led to a comprehensive functional and structural understanding of the VS ribozyme both in its *cis* and *trans* forms, which vary according to the covalent attachment of the stem-loop I (SLI) substrate domain [for reviews see (1,7–9)]. These studies have highlighted a unique mode of substrate recognition for the VS ribozyme, which involves specific recognition of the SLI domain in a folded hairpin state (10). Only a few studies have addressed the possibility of using the VS ribozyme to target and cleave RNA stem-loops that differ from the natural SLI substrate. In contrast, several other small nucleolytic ribozymes, particularly the hairpin, hammerhead and HDV ribozymes, have been modified to cleave numerous alternative single-stranded RNA substrates. For the VS ribozyme, the engineering principles that govern recognition of alternate substrates are likely more complex, but remain to be elucidated.

The catalytic domain or *trans* VS ribozyme (helical domains II–VI; Figure 1A) recognizes its hairpin substrate (SLI) via the formation of a kissing-loop interaction (KLI) required for efficient cleavage activity (10,11). In earlier work, mutagenesis and chemical modification studies provided evidence that this KLI contains three WC/WC (12) base pairs (bp) between loop I (G_{630}, U_{631} and C_{632}) and loop V (G_{697}, A_{698} and C_{699}), and that both loops likely form U-turn motifs (11). More recently, the nuclear magnetic resonance (NMR) structure of an SLI/SLV complex (13) and the crystal structure of the complete VS ribozyme (14) confirmed formation of the U-turn motifs and three *cis* WC/WC bp, but they also revealed the presence of a *cis* WC/sugar edge bp between C_{629} and A_{701} (between C_{10} of SLI and A_{14} of SLV in the SLI/SLV complex; Figure 1B). *In vitro* selection and biochemical studies of the VS ribozyme (15,16) as well as NMR studies of several SLI/SLV complexes (13) have provided evidence that formation of the I/V KLI is associated with a helix shift in the SLI substrate that is essential for catalysis. SLI variants that adopt a pre-shifted conformation bind with higher affinity to both the *trans* ribozyme (17) and an isolated SLV (18). Moreover, isothermal titration calorimetry (ITC) studies of SLI/SLV complexes conducted with a pre-shifted SLI RNA demonstrated that the I/V KLI is remarkably stable ($K_d = 0.24 \pm 0.02$ μM) and constitutes the predominant energetic contribution for substrate binding by the *trans* VS ribozyme (18). The I/V KLI is also important for substrate docking with

*To whom correspondence should be addressed. Tel: +1 514 343 7326; Fax: +1 514 343 2210; Email: pascale.legault@umontreal.ca

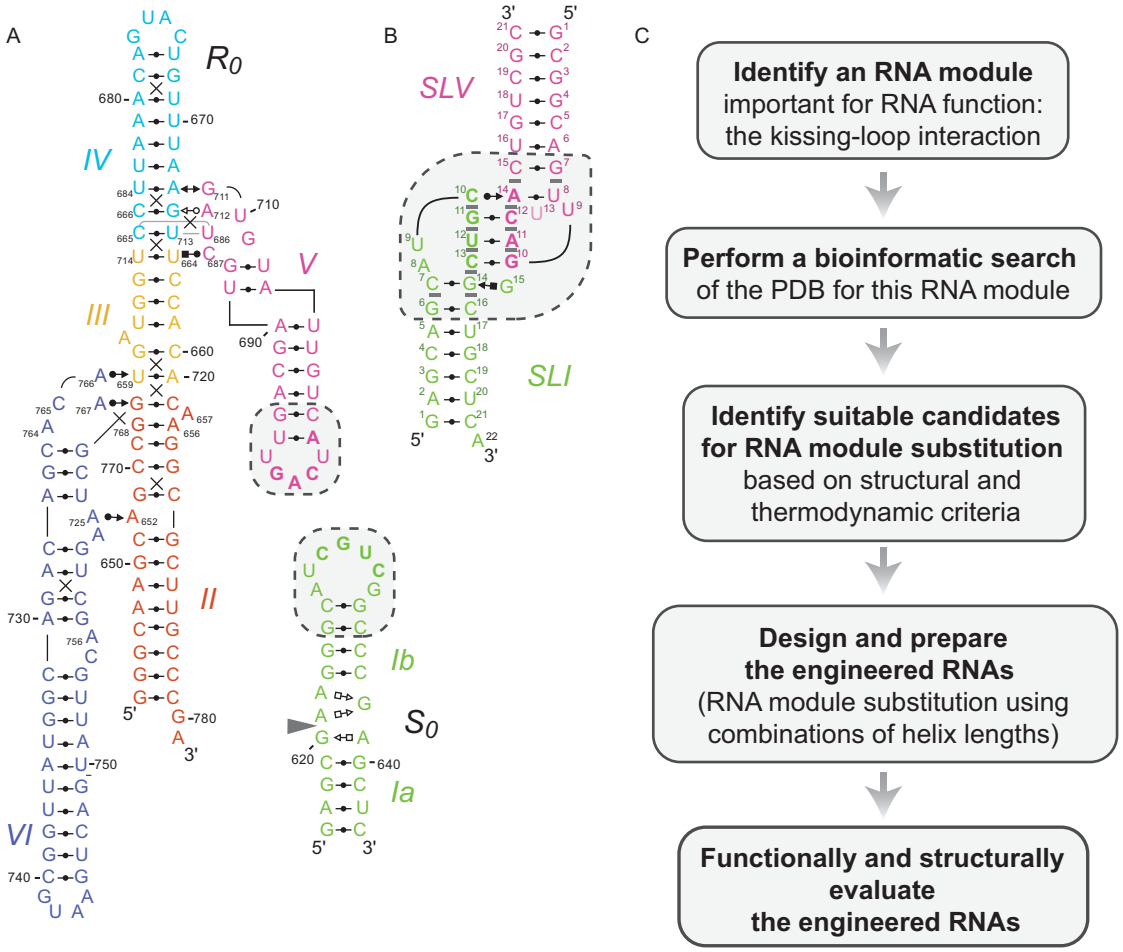

Figure 1. Rational engineering of KLIs for substrate recognition by the *Neurospora* VS ribozyme. (**A**) Structural schematic of a *trans* VS ribozyme system formed by the S_0 substrate and the R_0 ribozyme (32). The schematic is derived from NMR and X-ray structures (14,43). The cleavage site is located between G620 and A621 as indicated by the gray arrowhead. (**B**) Structural characteristics of the VS ribozyme I/V KLI derived from the NMR structure of the SLI/SLV complex [PDB ID: 2MI0; (13)]. (**C**) Flowchart of the engineering strategy used in this study. In (A and B), the dashed boxes enclose residues that contribute to the KLI and the closing base pairs of the two stems, whereas base-pairing interactions are represented using the Leontis-Westhof notation (12). In addition, base-pairing residues at the KLI are in bold. In (B), gray bars represent base stacking at the KLI.

the catalytic domain, which allows for the formation of the active site (19). In the proposed general acid-base mechanism of the VS ribozyme cleavage reaction, G_{638} from the internal loop of SLI (G_{638} loop) acts as the general base and A_{756} from the internal loop of SLVI (A_{756} loop) acts as the general acid (20–27). The recent crystal structure of the VS ribozyme confirms that the active site is formed through the association of these two internal loops, in which G_{638} and A_{756} are properly positioned with respect to the scissile phosphate to fulfill their proposed roles in catalysis (14).

Only a limited number of studies have investigated the possibility of using the VS ribozyme to selectively cleave RNA stem-loops other than its natural SLI substrate. Although minor changes to the sequence of the natural SLI substrate are compatible with VS ribozyme cleavage (11,15,28–31), larger sequence changes in the substrate may only be possible by incorporating compensating changes in the catalytic domain. To test this possibility, we recently investigated the cleavage of variant SLI substrates, in which the number of base pairs in stem Ib was either increased or decreased, using variant *trans* ribozymes containing a variable number of base pairs in stem V (32). We observed helix-length compensation between stem Ib and stem V, since the highest activity for each ribozyme variant was observed with a substrate that contains the compensatory number of base pairs in stem Ib (or one less). Moreover, this study establishes that VS ribozyme derivatives efficiently cleave SLI substrates that contain an alternate number of base pairs in stem Ib.

Given these encouraging results with the VS ribozyme, we were interested to gain further insights into the adaptability of this unique ribozyme for specific cleavage of folded RNA stem-loops. Previous studies have led to the idea that the I/V KLI of the VS ribozyme is an independent RNA module (13,16,18,31), and we hypothesized that this KLI can be substituted by other KLIs to create variant ribozymes that efficiently cleave stem-loop substrates with a modified terminal loop. In the present study, we developed a rational engineering approach to replace the I/V KLI of the *Neurospora* VS ribozyme by other KLIs and achieve efficient

substrate cleavage (Figure 1C). This rational approach is supported by the recently available NMR structure of an SLI/SLV complex (13) and the crystal structure of the complete VS ribozyme (14). We first performed a bioinformatic search for KLIs in the protein data bank (PDB), which allowed us to identify two KLIs that share structural characteristics with the natural KLI of the VS ribozyme. Next, VS substrate/ribozyme (S/R) pairs, in which the I/V KLI was substituted by each of these two KLI candidates, were prepared using several combinations of helix length for stems Ib and V (32) in order to fine-tune the structural context of the surrogate KLIs necessary to obtain efficient cleavage of the modified substrates. The engineered S/R pairs were then kinetically characterized to identify the most efficient ones and structurally evaluated to validate the procedure. Interestingly, several novel S/R pairs were identified that display substantial catalytic activity, further illustrating the adaptability of the VS ribozyme architecture for cleavage of alternate stem-loop substrates.

MATERIALS AND METHODS

Search for KLIs with WebFR3D

A bioinformatic search was performed with WebFR3D (33) to find KLIs in the PDB. The search query was defined as an interaction matrix between a set of 6 nt with no specific nucleotide identity (NT1 to NT6; Supplementary Figure S1B). Nucleotides NT1 and NT3 form a *cis* WC/WC base pair that closes the first loop, and this loop contains a non-self-pairing strand of 4–10 nt. Nucleotides NT4 and NT6 form a *cis* WC/WC base pair that closes the second loop, and this loop also contains a non-self-pairing strand of 4–10 nt. Nucleotides NT2 and NT5 are part of the first and second loops, respectively, and must form a *cis* WC/WC base pair. Finally, residues NT1-NT3 must be either sequentially located 5' respectively to residues NT4-NT6 or part of a different chain. For this search, we used the WebFR3D list of non-redundant RNA-containing structures determined by X-ray crystallography, Cryo-EM or NMR spectroscopy.

Clustering of WebFR3D results

A custom Python script was used to parse the HTML output file of WebFR3D. The script extracts two key features about each entry: the PDB ID of the associated structure and the type and numbering of the nucleotides (NT1-NT6) matching the query. It then uses this information to cluster all fragments associated with a single KLI and quantifies the number of *cis* WC/WC base pairs associated with this interaction.

Structural data retrieval and result listing

A custom Python script was used to automatically gather information about each KLI. The size of each loop and the total number of *cis* WC/WC base pairs in the KLI were retrieved directly from the cluster of WebFR3D results and used to define the secondary structure of each KLI. Additional information was retrieved from the RCSB repository via the PDB ID of the KLI. The information gathered about each KLI structure was listed as an HTML page enriched with JavaScript (Supplementary Figure S1D and Table S1).

Plasmids

The Avapl ribozyme (R_0, Figure 1A) is a derivative of the AvaI ribozyme and its parental plasmid (pAvapl) was constructed by polymerase chain reaction from the A-3 clone (10). The plasmids for transcription of the R_{TAR*}, R_{L22} and R_{L88} ribozyme variants (Figure 3A and Supplementary Figures S3A and 4A) were prepared by QuikChange II site-directed mutagenesis (Stratagene, CA, USA). All plasmids were validated by DNA sequencing.

ITC studies

Preparation of RNA and ITC studies were performed as previously described (18). Relevant experimental details are provided in the legend of Supplementary Figure S2.

Preparation of RNAs for kinetic studies

The R_{TAR*}, R_{L22} and R_{L88} ribozymes were prepared by *in vitro* T7 RNA polymerase transcription from plasmid templates linearized at the AvaI site. All ribozymes were purified by gel electrophoresis and ion-exchange HPLC, as previously described (32). The S_{TAR}, S_{L88} and S_{L22} substrates were synthesized *in vitro* using the T7 RNA polymerase and partially single-stranded synthetic oligonucleotide templates (Integrated DNA Technologies, IA, USA). These substrates were purified by gel electrophoresis, dephosphorylated with calf alkaline phosphatase and 5'-end-labeled with γ-(^{32}P) adenosine triphosphate (PerkinElmer, Ont.) using established procedures (32).

Kinetic studies

Mutiple-substrate and single-substrate kinetic studies were carried out as single-turnover reactions at 37°C in 1× Kinetic Reaction buffer (50 mM Tris at pH 7.6, 25 mM KCl, 2 mM spermidine and 25 mM $MgCl_2$), as previously described (32). Briefly, multiple-substrate kinetic studies were typically performed with a mixture of 5'-^{32}P-labeled nucleic acids containing all purified substrates for a given S/R pair (35 pM of each) and excess R (0.005–25 μM). These multiple-substrate kinetic studies were used to identify quickly the S/R pairs that lead to detectable substrate cleavage. All multiple-substrate kinetic experiments were performed at least three times.

Reactive S/R combinations were further investigated by single-substrate kinetic studies to derive the values of k_{obs} and k_{cat}/K_M. These studies were typically performed with $[S] = 250$ pM and excess R (0.005–15 μM). The percentage of remaining substrate [$F = S_t/(S_t + P_t) * 100\%$; where S_t and P_t are the amount of substrate and product at time t] was plotted against time. The resulting time courses were fit to the equation $F = Ae^{-(k_{obs} * t)} + F_\infty$, where A is the amplitude, k_{obs} is the rate of the reaction and F_∞ is a variable that represents the unreactive fraction of the substrate. The value of k_{obs}, the standard error for k_{obs} and the F_∞ parameter were estimated by non-linear regression analysis within the OriginPro 8.1 software (OriginLab, MA, USA). The F_∞ values are below 10% for all S/R combinations. A linear dependence of k_{obs} on [R] was observed for each S/R

combination at the lowest values of [R] and analyzed by linear regression to derive the second order rate constant of the reaction, k_{cat}/K_M. The quality of the fit for the linear dependence of the k_{obs} on [R] was obtained from the square of the correlation coefficient (R^2), and in all cases R^2 was ≥ 0.99. For the single-substrate kinetic experiments, three independent experiments were performed, and reported k_{cat}/K_M and their errors are average values and standard deviations, respectively, from these multiple measurements.

Native gel studies of RNA substrates

Non-denaturing polyacrylamide gel electrophoresis was carried out on a 7.5% polyacrylamide bisacrylamide (37.5:1) gel in Tris-glycine buffer (25 mM Tris pH 8.0 and 200 mM glycine). Prior to loading, the RNA substrates (1 and 4 μg) were heated at 95°C for 2 min in storage buffer [10 mM Tris pH 7.6 and 1 mM ethylenediaminetetraacetic acid (EDTA)] and transferred on ice for 5 min. Then, 4 μl of 2× Kinetic Reaction buffer was added and the samples were incubated at 37°C for 5 min. The gel was pre-run for 30 min at 100 V, run for 2 h at 250 V and 4°C and then stained with Stains All (Sigma-Aldrich, Ont.).

SHAPE studies of ribozymes

For SHAPE (Selective 2'-hydroxyl Acylation analyzed by Primer Extension) experiments, variant ribozymes (20 pmol) in 4 μl of H_2O were first incubated at 37°C for 5 min with 5 μl of 2× Kinetic Reaction buffer and then treated with 1 μl of 130 mM *N*-methylisatoic anhydride (NMIA; dissolved in anhydrous dimethyl sulfoxide). The resulting mix was incubated for 54 min at 37°C and then transferred on ice. Reverse transcription reactions were performed on mutant ribozymes with 5'-^{32}P-labeled primers and SuperScript III reverse transcriptase (ThermoFisher Scientific Inc.), as previously described (34). The primer extension products were separated on an 8% denaturing polyacrylamide gel (7 M urea, 90 mM Tris/Borate, 2 mM EDTA). The gel was visualized by phosphorimager (Personal Molecular Imager™ System, Bio-Rad) and quantified using Image Lab Software 4.1.

Three-dimensional modeling of S/R complexes with a substituted KLI

Models of the S_0/R_0, $S_{L88\text{-}0}/R_{L22\text{-}0}$ and $S_{TAR\text{-}0}/R_{TAR*\text{-}0}$ complexes were constructed by fragment assembly in PyMOL (The PyMOL Molecular Graphics System, Version 1.7.4 Schrödinger, LLC.) based on heavy-atom superpositions with the S_X/R_X complex obtained from the X-ray structure of the VS ribozyme [PDB ID: 4R4P; (14)] by taking the SLI substrate of one protomer (S_X) and the *trans* VS ribozyme (helical domains II–VI) of the other protomer (R_X). Starting with representative high-resolution structures of the studied KLIs [PDB ID: 2MI0—model 2 (13)], 1KIS—model 2 (35) and 4IOA (36)], the hairpin stems within these complexes were modified by stems generated with MC-Sym (37) that match those of SLI (residues 623–626 and 634–637) and SLV (residues 688–694 and 702–708) from the S_0/R_0 complex (Figure 1A), and the resulting hybrid structures retained the hairpin loop residues of the original high-resolution structures (2MI0: residues 4–17 and 104–118; 1KIS: residues 5–12 and 21–28; and 4IOA: residues 423–430 and 2383–2392). The hairpin stem corresponding to stem V within these hybrid structures was superposed to stem V of R_X. Subsequently, S_X was copied one time for each hybrid structure and its stem Ib was superposed to stem Ib of each hybrid structure. The final S/R complexes retain all residues from the hybrid structures, all residues of R_X except for residues 688–708 of SLV and only residues 616–622 and 638–643 of S_X (according to residue numbering in Figure 1).

RESULTS

Search for KLIs in the PDB

We searched for three-dimensional structures of KLIs in the PDB using a three-step computational workflow (Supplementary Figure S1A) that is based on the motif-search tool WebFR3D (33). This online version of the FR3D program was chosen because it has the capacity to perform searches of RNA motifs composed of non-contiguous nucleotides in a curated ensemble of non-redundant structures. In the first step, a search query was launched with WebFR3D to identify single *cis* Watson–Crick (WC) base pairings between any two residues belonging to two different terminal loops of 4–10 residues in length (Supplementary Figure S1B). This search used the WebFR3D list of non-redundant RNA-containing structures determined by X-ray crystallography, Cryo-EM or NMR spectroscopy. In the second step, the individual entries of the WebFR3D output were clustered to identify all existing WC pairings for a specific pair of terminal loops, and thereby provide a list of KLIs. In the third and final step, additional structural data and related information were retrieved for each KLI, and these data were listed in an interactive HTML/JavaScript table (Supplementary Figure S1D and Table S1). From this motif search of the PDB, 113 KLIs were identified and these form between one and ten *cis* WC/WC base pairs at the kissing-loop interface.

Selection of KLIs that could substitute for the VS ribozyme I/V interaction

To identify KLIs that could substitute for the VS ribozyme I/V KLI, we automatically filtered the list of 113 structures to eliminate all entries originating from X-ray and Cryo-EM structures with resolution ≥3.6 Å and only selected those that form heterodimeric KLI interactions with 3–10 *cis* WC/WC base pairs. Heterodimeric KLIs were selected because substitutions of SLI and SLV in the VS ribozyme S/R system (Figure 1A) by stem-loops that form an homodimeric KLI might lead to self-association of substrates and ribozymes, which could interfere with *trans* cleavage. In addition, KLIs with a minimum of three *cis* WC/WC base pairs were selected to prevent formation of an unstable KLI that could lead to inefficient *trans* cleavage (11,31). This filtering step produced a list of 17 structures that represent 6 types of KLIs (Table 1): the TAR/TAR* interaction derived from HIV-1; the L6/L7 and L22/L88 interactions from the large subunit of rRNAs; the L5/L13 interaction from the cobalamin riboswitch; the L3/L4 interaction from

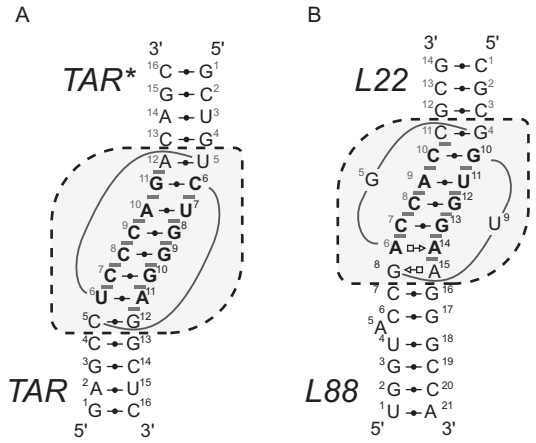

C

Complex	K_d (μM)
SLI/SLV	0.24 ± 0.02
*TAR/TAR**	0.0059 ± 0.0005
L22/L88	3.8 ± 0.5

Figure 2. Schematics and thermodynamic stability of selected KLIs. Structural characteristics of the selected KLIs: (**A**) the HIV-1 TAR/TAR* KLI [PDB ID**:** 1KIS; (35)] and (**B**) the large ribosomal subunit L22/L88 KLI from *Deinococcus radiodurans* [PDB ID: 4IOA; (36)]. (**C**) Dissociation constants (K_d) of the selected KLIs determined in a previous study for the SLI/SLV and TAR/TAR* complexes (18) and here for the L22/L88 complex (Supplementary Figure S2). These K_d values were all determined at 25°C in 10 mM Tris pH 7.0 and 20 mM $MgCl_2$. In (A and B), the dashed boxes enclose residues of the KLI and the closing base pairs of the two stems and base-pairing interactions are represented using the Leontis-Westhof notation (12). In addition, base-pairing residues at the KLI are in bold and gray bars highlight base stacking at the KLI.

the human SRP Alu domain; and the ColE1 KLI. To identify suitable KLIs for our engineering studies, we selected those that share structural similarities with the VS ribozyme I/V KLI. More specifically, a suitable KLI must fit certain structural characteristics: (i) form consecutive *cis* WC/WC base pair with non-modified nucleotides, (ii) the adjoining stems must contain at least three consecutive *cis* WC/WC base pairs and (iii) the interhelical angle must fall between 125° and 175° (13,38). Such structural criteria limited our choice to two classes of KLIs: the HIV-1 TAR/TAR* interaction and the L22/L88 (loop 22/loop 88) interaction from the large subunit of rRNAs, and those with PDB ID codes 1KIS (35) and 4IOA (36) were selected for our engineering studies.

Thermodynamic stability of the selected KLIs

To ascertain that the two selected KLIs are good candidates for our engineering studies, we verified their thermodynamic stability. Although the TAR/TAR* and L22/L88 KLIs incorporate a larger number of WC base pairs than the VS ribozyme I/V KLI (Figures 1B and 2A and B), the latter is known to be exceptionally stable (18). Based on ITC studies, the K_d of the TAR/TAR* and L22/L88 complexes are 40-fold lower and 16-fold higher, respectively, than that of the SLI/SLV complex (Figure 2C and Supplementary Figure S2). These results confirm that the thermodynamic stability of the two selected KLIs is not considerably different from that of the I/V KLI. Thus, these two KLIs were considered suitable for our engineering studies.

Kinetic characterization of VS ribozyme *S*/*R* pairs with a modified I/V KLI

Next, kinetic studies were performed to test the hypothesis that the two selected KLIs can substitute for the natural I/V KLI interaction and yield active VS ribozyme variants. For these studies, we used the previously-characterized S_0/R_0 pair formed between a pre-shifted SLI substrate and a *trans* VS ribozyme (32). Since the selected KLIs may functionally replace the I/V KLI only when substituted in the proper orientation (e.g. either the L22 or the L88 loop replacing loop I) and with supporting helices of proper lengths, we prepared three combinatorial pools of *S*/*R* pairs that consist of 25 S_{TAR}/R_{TAR*} pairs, 30 S_{L88}/R_{L22} pairs and 36 S_{L22}/R_{L88} pairs (Figure 3A and Supplementary Figures S3A and 4A). Within each pool, helix-length variations were introduced in both stem Ib of the variant substrates (S_{TAR}, S_{L88} and S_{L22}) and stem V of the variant ribozymes (R_{TAR*}, R_{L22} and R_{L88}). In this context, compensatory *S*/*R* pairs are those for which the total number of base pairs in stems Ib and V is identical to that found for the S_0/R_0 reference pair (Figure 1). For all *S*/*R* combinations, the second-order rate constant k_{cat}/K_M was determined under single turnover conditions. It is important to note that the catalytic parameter k_{cat}/K_M is very useful when comparing the relative activity of a given enzyme for different competing substrates (e.g. R_{TAR*-0} acting on the different S_{TAR} substrates), but may be misleading when comparing the relative activity of different enzymes (39), particularly those of different *S*/*R* families. Thus, to compare the catalytic activity of different *S*/*R* families, we also relied on the values of the cleavage rate constant (k_{obs}) measured under identical experimental conditions.

Kinetic studies of the VS ribozyme S_{TAR}/R_{TAR*} pairs

Single turnover kinetic studies were performed to derive the second-order rate constant k_{cat}/K_M for all 25 S_{TAR}/R_{TAR*} combinations. ^{32}P-labeled S_{TAR} substrates were cleaved with an excess of R_{TAR*} ribozymes, and the cleavage reaction monitored by denaturing gel electrophoresis. Initially, we used a multiple-substrate kinetic approach, where one enzyme is simultaneously incubated with a mixture of substrates (32). Given that the substrates are of different sizes (Figure 3A), the fate of any given substrate can be monitored by gel electrophoresis (32). For several of the S_{TAR}/R_{TAR*} combinations, no cleavage activity was detected after 24 min at $[R] \leq 15$ μM ($k_{obs} \leq 0.002$ min^{-1}; light gray shading in Figure 3B). For the remaining S_{TAR}/R_{TAR*} combinations that displayed detectable cleavage activity, a single-substrate kinetic approach was used to precisely derive k_{cat}/K_M values. The highest k_{cat}/K_M value (0.53 ± 0.03 min^{-1}μM^{-1}) was obtained for the $S_{TAR\text{-}1}/R_{TAR*\text{-}0}$ combination (Figure 3B), which is 46-fold lower than that of S_0/R_0 ($k_{cat}/K_M = 24.5 \pm 0.9$ min^{-1}μM^{-1} at 37°C; data not

Table 1. Filtered results of the bioinformatics search to identify KLIs from the PDB

Interaction Class	Organism	PDB ID codes	Experimental method (Resolution in Å)	Structural characteristics of the KLI[a]		
				WC Pairs	Size of loops	Inter-helical Angle
HIV-1 TAR/TAR*	Synthetic	2JLT	X-ray (2.90)	6	6 / 8	160˚
		2RN1	NMR	6	6 / 8	125˚ ± 1˚
		1KIS	NMR	6	6 / 6	136˚
		2PN9[b]	NMR	6	6 / 8	155˚ ± 5˚
L6/L7 of rRNA large subunit	*Thermus thermophilus*	3V2F	X-ray (2.70)	4	8 / 7	94˚
	Escherichia coli	2QBG	X-ray (3.30)	4	8 / 7	93˚
	Deinococcus radiodurans	4IOA	X-ray (3.20)	4	8 / 7	n/a
	Haloarcula marismortui	1S72	X-ray (2.40)	4	8 / 7	78˚
L22/L88 of rRNA large subunit	*Thermus thermophilus*	3V2F	X-ray (2.70)	4	6 / 8	137˚
	Escherichia coli	2QBG	X-ray (3.30)	4	6 / 8	146˚
	Deinococcus radiodurans	4IOA	X-ray (3.20)	4	6 / 8	152˚
	Haloarcula marismortui	1S72	X-ray (2.40)	6	7 / 7	154˚
	Tetrahymena thermophila	4A1B	X-ray (3.52)	6	8 / 7	139˚
	Saccharomyces cerevisiae	3U5H	X-ray (3.00)	6	8 / 7	154˚
L5/L13 of cobalamin riboswitch	Marine Metagenome	4FRN	X-ray (3.43)	5	6 / 8	n/a[a]
L3/L4 of SRP Alu domain	*Homo sapiens*	1E8O	X-ray (3.20)	3	6 / 8	68˚
ColE1 RNAI/RNAII	Synthetic	2BJ2	NMR	7	7 / 7	119˚

[a]Each structure was analyzed with the PyMOL Molecular Graphics System (Version 1.3, Schrödinger) to identify the number of *cis* WC/WC base pair and size of loops at the KLI and with Curves+ (38) to measure the interhelical angle between the stems connecting a specific KLI. Interhelical angles were measured only for the KLIs where the adjoining stems contain a minimum of three base pairs, and are not available (n/a) for the other KLIs.
[b]Contains modified nucleotides at the KLI.

shown). Several other S_{TAR}/R_{TAR*} combinations have similar catalytic efficiency (within 5-fold; dark gray shading in Figure 3B), and these combinations involve all five R_{TAR*} ribozymes and four of the five S_{TAR} substrates.

For R_{TAR*-0}, efficient substrate cleavage is obtained with S_{TAR-1} as well as with S_{TAR-0}, indicating limited substrate promiscuity. Other R_{TAR*} ribozymes also display similar specificity, cleaving efficiently only two to three out of the five S_{TAR} substrates. Given that the highest k_{cat}/K_M values for each ribozyme is observed with the compensatory substrate or one that varies by one or two base pairs, it can be concluded that efficient substrate cleavage depends on helix-length compensation in stem V of the variant ribozyme. For example, the optimal ribozyme for S_{TAR-1} is R_{TAR*-0}, whereas the optimal one for S_{TAR+2} is R_{TAR*-3}. Thus, for the S_{TAR}/R_{TAR*} family, there is limited substrate promiscuity for all ribozymes as well as helix-length compensation across the family, as previously observed for the reference S/R family (32).

Kinetic studies of the VS ribozyme S_{L88}/R_{L22} and S_{L22}/R_{L88} pairs

In a similar manner, multiple and single turnover kinetic studies were performed to evaluate the k_{cat}/K_M of the 30 S_{L88}/R_{L22} and 36 S_{L22}/R_{L88} combinations (Supplementary Figures S3 and 4). For the S_{L88}/R_{L22} pairs, the most active combination is S_{L88+1}/R_{L22-1} with a k_{cat}/K_M of 0.39 ± 0.03 min^{-1} μM^{-1}, which is 63-fold lower than that of S_0/R_0. A few other S_{L88}/R_{L22} combinations produce similar k_{cat}/K_M (within 5-fold; dark gray shading in Supplementary Figure S3B), and these combinations involve three of the five S_{L88}substrates and three of the six R_{L22} ribozymes. Each of these three ribozymes displays similar cleavage activity for one or two S_{L88} substrates, and helix-length com-

A

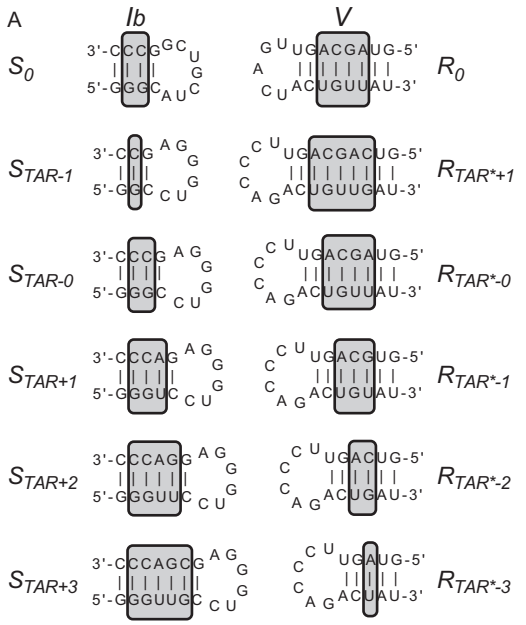

B

	R_{TAR*-3}	R_{TAR*-2}	R_{TAR*-1}	R_{TAR*-0}	R_{TAR*+1}
S_{TAR-1}	n.d.	n.d.	10 ± 2	53 ± 3	19.1 ± 0.5
S_{TAR-0}	n.d.	11 ± 1	10 ± 3	11.2 ± 0.6	4.6 ± 0.3
S_{TAR+1}	34 ± 6	25 ± 4	4.3 ± 0.2	n.d.	n.d.
S_{TAR+2}	26 ± 1	3.2 ± 0.5	n.d.	n.d.	n.d.
S_{TAR+3}	n.d.	n.d.	n.d.	n.d.	n.d.

Figure 3. Sequences and kinetic data of the S_{TAR}/R_{TAR*} variants. (**A**) Sequences of the S_{TAR}/R_{TAR*} variants. Only the regions of the S_0 substrate and R_0 ribozyme (stem-loops Ib and V shown above; Figure 1A) that were substituted in the S_{TAR} and R_{TAR*} variants are shown. The number of base pairs varies in stems Ib and V, as indicated by the gray boxes on the putative secondary structures. (**B**) Grayscale heat map of the k_{cat}/K_M values (10^{-2} $min^{-1}\mu M^{-1}$) for the S_{TAR}/R_{TAR*} variants. Dark gray shading corresponds to k_{cat}/K_M values within 5-fold of the most active S_{TAR}/R_{TAR*} pair (S_{TAR-1}/R_{TAR*-0}); medium gray shading corresponds to lower k_{cat}/K_M values (5–17-fold lower than the most active S_{TAR}/R_{TAR*} pair), and light gray shading reflects the absence of detectable cleavage activity (n.d.: $k_{obs} \leq 0.002$ min^{-1}) after 24 min at $[R] \leq 15$ μM.

pensation is observed given that the most active S_{L88}/R_{L22} combinations for these ribozymes are the $S_{L88\text{-}0}/R_{L22\text{-}0}$, $S_{L88+1}/R_{L22\text{-}1}$ and $S_{L88+2}/R_{L22\text{-}2}$ pairs. For the S_{L22}/R_{L88} pairs, the highest k_{cat}/K_M obtained is 0.23 ± 0.02 min^{-1} μM^{-1} for $S_{L22+1}/R_{L88\text{-}1}$, which is 107-fold lower than that of S_0/R_0. In contrast to the S_{L88}/R_{L22} combinations, several S_{L22}/R_{L88} combinations display similar catalytic activity (within 5-fold; dark gray shading in Supplementary Figure S4B), and these combinations involve four of the six S_{L22} substrates and five of the six R_{L88} ribozymes. For each of the five active ribozymes, comparable k_{cat}/K_M values are obtained with one to four of the six S_{L88} substrates, indicating different degrees of substrate promiscuity. Furthermore, helix-length compensation is observed for all variant ribozymes given that the highest k_{cat}/K_M values for each ribozyme is observed with the compensatory substrate or one that varies by one base pair. For example, the optimal substrate for R_{L88+1} is S_{L22+0}, whereas the optimal one for $R_{L88\text{-}4}$ is S_{L22+4}. Thus, for both the S_{L88}/R_{L22} and S_{L22}/R_{L88} families, there is limited substrate promiscuity for all ribozymes as well as helix-length compensation across the family, as previously observed for the reference S/R family (32).

Comparison of the catalytic activity of the different S/R families

Given that k_{cat}/K_M values can be misleading when comparing the relative activity of the various S/R families, we also compared the k_{obs} values for the S/R pair of each family that displays the highest catalytic activity. These k_{obs} values, determined under identical single turnover conditions, indicate that the activities of the S_{TAR}/R_{TAR*}, S_{L88}/R_{L22} and S_{L22}/R_{L88} family representatives are reduced by 159-, 53- and 84-fold, respectively, compared to the parental S_0/R_0 pair (Supplementary Table S2). Thus, although both the k_{cat}/K_M and k_{obs} values indicate that there is a significant level of catalytic activity for some variant S/R pairs, their activity is still lower than that of the parental S_0/R_0 pair.

Structural characterization of the variant substrates

To insure that the variant substrates examined in this study are properly folded, these substrates were analyzed by native gel electrophoresis. The migration of variant substrates on native gels was compared with that of two previously investigated VS ribozyme substrates (32), $S_{-1\ bp}$ and $S_{-2\ bp}$, which respectively adopt a hairpin and a duplex conformation. Our results show that all variant substrates migrate on a native gel in a manner similar to the active hairpin conformation (Supplementary Figure S5).

Structural characterization of the variant ribozymes

To verify the proper folding of variant ribozymes, the secondary and tertiary structures of these *trans* ribozymes were analyzed by SHAPE experiments. In these studies, the reactivity of each nucleotide to NMIA is quantified and interpreted as being directly linked to the local nucleotide flexibility (34). For the R_{TAR*-0} ribozyme (Figure 4), the nucleotides reactive to NMIA are found in non-helical regions that are likely to be dynamic, including the A_{718} and $A_{725}A_{726}$ bulges, the A_{756} loop and the terminal loops of stem-loops IV, V and VI (40–43). The reactivity patterns

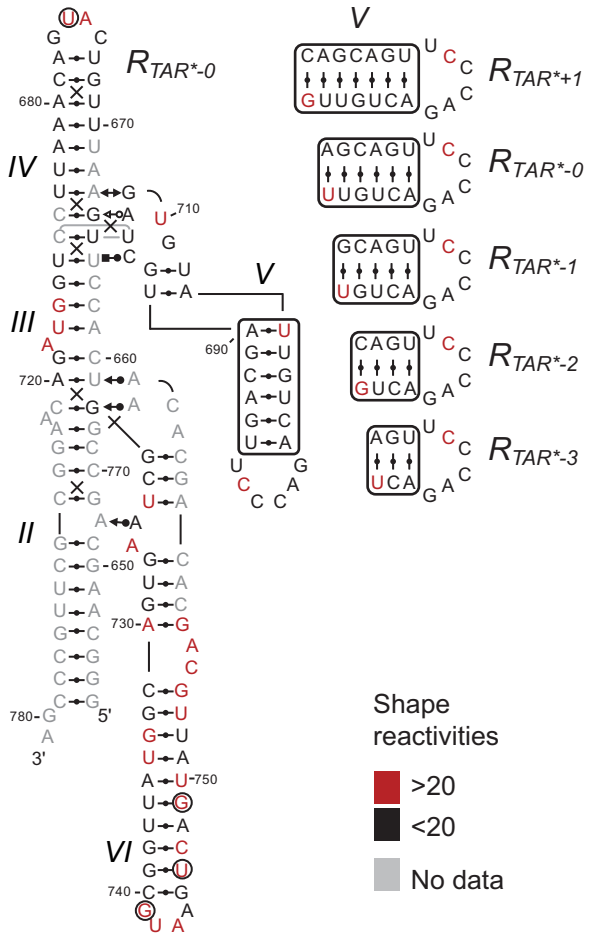

Figure 4. SHAPE analysis of the R_{TAR*} ribozyme variants. The normalized NMIA reactivity of each nucleotide within R_{TAR*-0} is color-coded on its structural schematic as per the SHAPE reactivities key. For the other R_{TAR*}variants, the normalized NMIA reactivity is within the same category as for R_{TAR*-0}, except for a few nucleotides in the variable SLV region (right panel) and outside this region (black circles indicate inverted reactivity compared to R_{TAR*-0}; U_{675} for R_{TAR-1} and G_{741}, U_{746} and G_{749} for R_{TAR-3}).

of the other R_{TAR*} ribozymes are very similar to that of the R_{TAR*-0} ribozyme (Figure 4). In addition, the reactivity patterns of the R_0, R_{L22} and R_{L88} ribozymes are similar to those of the R_{TAR*} ribozymes in that known helical regions display lower reactivity to NMIA compared to non-helical regions (Supplementary Figure S6). As an exception, residues within and adjacent to G-U base pairs (in stem-loops V and VI) produce idiosyncratic patterns of NMIA reactivity, as previously demonstrated (44). Of note, the most NMIA-reactive nucleotide in all ribozymes is A_{726}, an extruded residue from the II-VI bulge-bulge interaction and the most disordered residue in the NMR structures of the II-III-VI junction (14,43,45). Overall, the SHAPE results for all of the engineered ribozymes are in good agreement with the structural schematics of the R_0 ribozyme derived from NMR and X-ray structures [Figure 1; (14,43)]. Thus, all of the variant VS ribozymes investigated here adopt a ground state conformation that is compatible with cleavage activity.

Structural modeling of the S_0/R_0, $S_{L88\text{-}0}/R_{L22\text{-}0}$ and $S_{TAR\text{-}0}/R_{TAR*\text{-}0}$ pairs

Once a stable KLI is formed between a well-folded VS ribozyme variant and its stem-loop substrate, the G_{638} internal loop of the substrate must properly interact with the A_{756} loop of the ribozyme to allow formation of a productive active site. In order to assess the effect of substituting the I/V KLIs on formation of the VS ribozyme active site, three-dimensional models of the $S_{L88\text{-}0}/R_{L22\text{-}0}$ and $S_{TAR\text{-}0}/R_{TAR*\text{-}0}$ pairs were produced. These models were built by fragment assembly, combining either the X-ray structure of the L22/L88 KLI or the NMR structure of the TAR/TAR* KLI with the X-ray structure of the VS ribozyme [Figure 5; (14,35,36)]. As a control, the model of the S_0/R_0 pair was similarly built from the NMR structure of the SLI/SLV complex. In contrast with the close state observed in the X-ray structure (Figure 5B), the model of the S_0/R_0 pair (Figure 5C) adopts an open state with the G_{638} loop of SLI apart from the A_{756} loop of SLVI. This is not surprising, since the open state, previously described in the NMR-based model of the complete VS ribozyme, likely represents a ground-state conformation of the S/R complex (43). In the S_0/R_0 model, the scissile phosphate within the G_{638} loop is 26.6 Å from the corresponding phosphate in the crystal structure, but oriented directly toward A_{756}, such that a simple repositioning of the helical domains containing the G_{638} and A_{756} loops would allow formation of the active site. The models of both the $S_{L88\text{-}0}/R_{L22\text{-}0}$ (Figure 5D) and $S_{TAR\text{-}0}/R_{TAR*\text{-}0}$ pairs (Figure 5E) also represent an open state of the ribozyme with their scissile phosphates respectively 23.0 Å and 31.9 Å from the corresponding phosphate within the crystal structure. However, in both these models, the scissile phosphate is not oriented favorably with respect to the A_{756} loop to facilitate formation of the active site. Overall, these models suggest that substitutions of the KLI in the variant S/R pairs may reduce the probability of encounter between the G_{638} internal loop of the substrate and the A_{756} loop of the ribozyme and thus likely impair both the formation of the active site and the subsequent cleavage reaction.

DISCUSSION

In this work, a comprehensive RNA engineering approach was developed, which demonstrates that the I/V KLI of the VS ribozyme is an RNA module that can be substituted by other KLIs while maintaining efficient substrate cleavage. Several KLIs were initially identified through a bioinformatics search of the PDB, of which two were selected as being structurally similar to the I/V KLI of the VS ribozyme: the HIV-1 TAR/TAR* KLI [PDB ID: 1KIS; (35)] and the L22/L88 KLI from the large subunit of rRNAs [PDB ID: 4IOA; (36)]. These two KLIs were substituted for the I/V KLI of the S_0/R_0 reference pair formed between a pre-shifted substrate and a *trans* version of the VS ribozyme. In addition, a combinatorial approach was used in which several variant S/R pairs were synthesized that contain different helix lengths in stems Ib and V. The resulting S/R pairs were kinetically evaluated, and several show substantial catalytic activity. Below, we compare the catalytic properties of the most active variant S/R pairs with that of the previously

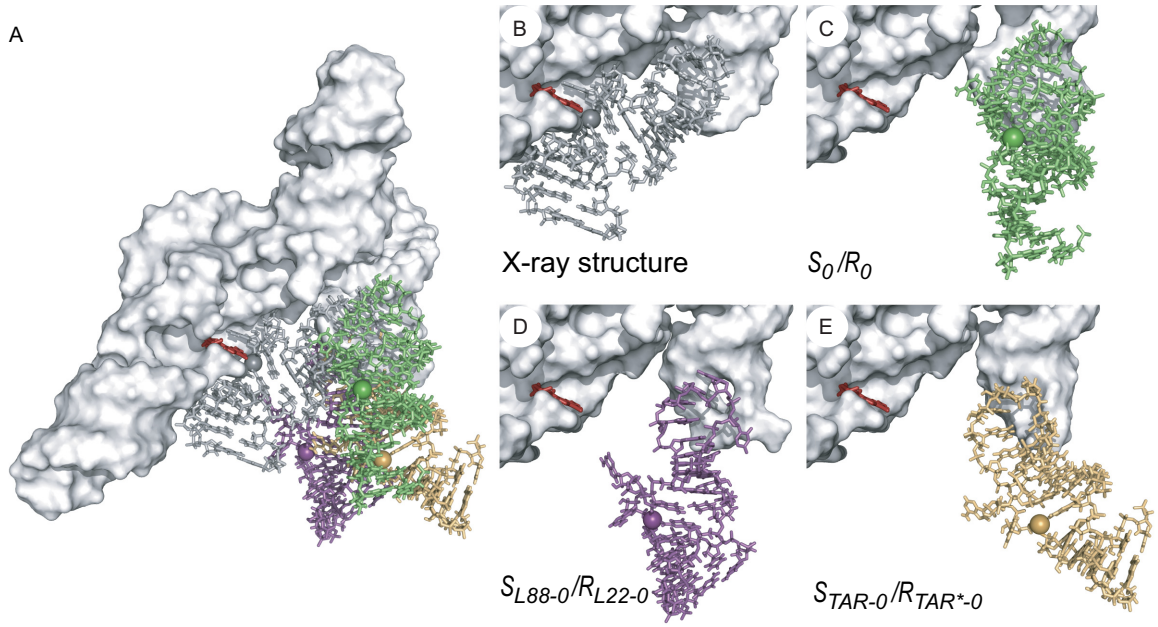

Figure 5. Three-dimensional models of substrate/ribozyme complexes. (**A**) Superposition of three-dimensional models of the variant S/R pairs on the X-ray structure of the VS ribozyme. Individual representations from this superposition are zoomed in and described in details for the subsequent panels. (**B**) X-ray structure of the VS ribozyme [PDB ID: 4R4P; (14)]. In this representation, the substrate of one protomer is shown in dark gray sticks with the phosphorus at the scissile phosphate as a sphere and the *trans* VS ribozyme (helical domains II–VI) of the other protomer is shown as a white surface, except for residue A_{756}, which is shown as red sticks. (**C**) Model of the S_0/R_0 pair derived from the NMR structure of a VS ribozyme SLI/SLV complex [lime green; PDB ID: 2MI0; (13)]. (**D**) Model of the $S_{L88\text{-}0}/R_{L22\text{-}0}$ pair derived from the X-ray structure of the ribosomal L22/L88 KLI [purple; PDB ID: 4IOA; (36)]. (**E**) Model of the $S_{TAR\text{-}0}/R_{TAR*\text{-}0}$ pair derived from the NMR structure of the TAR/TAR* complex [mustard yellow; PDB ID: 1KIS; (35)]. In (A–E), the *trans* VS ribozyme is shown as a white surface with A_{756} in red sticks and the individual substrates are shown as sticks with the phosphorus at the scissile phosphate as a sphere.

investigated S_0/R_0 pair in light of the thermodynamic and structural properties of the parental and surrogate KLIs.

Within the three families of S/R pairs investigated (S_{TAR}/R_{TAR*}, S_{L88}/R_{L22} and S_{L22}/R_{L88}), several S/R combinations show substantial catalytic efficiency (dark gray shading in Figure 3B and in Supplementary Figures S3B and 4B). For each family, helix-length compensation was observed for the most active S/R pairs, and this is consistent with what was observed in previous studies of the parental S_0/R_0 pair (32). For the S_{TAR}/R_{TAR*} family, the *trans* VS ribozyme variants can efficiently cleave an SLI substrate with stem Ib lengths of 3–6 bp (Figure 3B). Both the S_{L88}/R_{L22} and S_{L22}/R_{L88} families also allow an appreciable level of catalytic efficiency for several SLI substrates, with a stem Ib length of 4–7 bp for S_{L22}/R_{L88} and 4–6 bp for S_{L88}/R_{L22} (Supplementary Figures S3 and 4). Within the three families of S/R pairs investigated, the $S_{TAR\text{-}1}/R_{TAR*\text{-}0}$, $S_{L88+1}/R_{L22\text{-}1}$ and $S_{L22+1}/R_{L88\text{-}1}$ show the highest k_{cat}/K_M values, all within 2.5-fold of each other (0.2–0.5 $min^{-1}\mu M^{-1}$). Although these S/R pairs with surrogate KLIs behave like the reference S_0/R_0 pair in some respects, their k_{cat}/K_M values are reduced by 50- to 100-fold compared to S_0/R_0. Similarly, their k_{obs} values determined under identical conditions are reduced 50- to 160- fold compared to S_0/R_0. The KLIs most likely form and assist catalysis for the highly-active variant S/R pairs, given that several other variant S/R pairs within the same family are inactive and that disruption of the KLI in the parental S_0/R_0 pair can lead to more than a 1,000-fold decrease in k_{cat}/K_M and more than a 6000-fold decrease in k_{obs} (32). In addition, we verified by native gel electrophoresis and SHAPE analysis that all substrates and ribozymes of the variant S/R pairs adopt a stable fold equivalent to S_0 and R_0, respectively, and compatible with high catalytic efficiency. Thus, although surrogate KLIs allow high catalytic efficiency for some variant S/R pairs, it is puzzling that they do not allow the same high level of activity as that observed for the parental S_0/R_0 pair.

We have previously shown that mutations that decrease the affinity of the I/V KLI also lead to lower k_{cat}/K_M values when monitoring the *trans* cleavage reaction as done here (18,31). For example, deletion of U700 in SLV causes a 210-fold decrease in binding affinity for SLI and 140-fold decrease in k_{cat}/K_M (18,31). Thus, it is likely that the lower relative affinity of a surrogate KLI may affect the level of catalytic efficiency that could be attained in the variant S/R pairs. Given that the L22/L88 KLI is 16-fold less stable than the I/V KLI [Figure 2C; (18)], its higher K_d could explain in part the lower k_{cat}/K_M of the S_{L88}/R_{L22} (>60-fold) and S_{L22}/R_{L88} pairs (>100-fold) compared to S_0/R_0. However, given that the HIV-1 TAR/TAR* KLI is 40-fold more stable than the I/V KLI [Figure 2C; (18)], the difference in K_d of the KLI complex cannot explain the lower k_{cat}/K_M of the S_{TAR}/R_{TAR*} pairs (>50-fold) compared to S_0/R_0.

The VS ribozyme S/R pairs likely adopt both an open state and a close state that can be respectively represented by

the recent NMR-based model and X-ray structure (14,43). The KLI is stably formed in both states, but only the close state captures the active site formed by the association of the G_{638} and A_{756} loops. In order to assess the effect of substituting the I/V KLI on formation of the VS ribozyme active site, the S_0/R_0, $S_{L88\text{-}0}/R_{L22\text{-}0}$ and $S_{TAR\text{-}0}/R_{TAR*\text{-}0}$ pairs were modeled based on high-resolution structures of KLIs and the S/R complex derived from the X-ray structure of the VS ribozyme (Figure 5). Since all the modeled S/R pairs adopt an open state with the G_{638} loop apart from the A_{756} loop, it is difficult to precisely evaluate the compatibility of surrogate KLIs for formation of the active site. Nevertheless, we find that the distance between the scissile phosphates of the model and the crystal structure is longer for the $S_{TAR\text{-}0}/R_{TAR*\text{-}0}$ pair than for the S_0/R_0 and $S_{L88\text{-}0}/R_{L22\text{-}0}$ pairs. In addition, it appears from these models that formation of the active site from the open state would involve the simple packing of two helical domains for the S_0/R_0 pair, but possibly be more restrained for the $S_{L88\text{-}0}/R_{L22\text{-}0}$ and $S_{TAR\text{-}0}/R_{TAR*\text{-}0}$ pairs. Thus, the HIV-1 TAR/TAR* KLI and possibly the L22/L88 interaction, which both contain more base pairs than the I/V KLI, may partially restrict formation of the active site due to topological constraints. We envision that additional mutations of the VS ribozyme could be introduced to help compensate for such structural restriction and thereby increase the catalytic efficiency of the variant S_{L88}/R_{L22} and S_{TAR}/R_{TAR*} pairs.

Previous NMR studies of an SLI/SLV complex indicate that both the SLI and SLV loops contain several dynamic residues that could confer a certain degree of flexibility to the I/V KLI (13). Thus, the I/V KLI likely acts as a dynamic hinge that facilitates formation of the active site. It is not clear at this time if the surrogate KLIs allow the same degree of flexibility, and how their dynamics affect formation of the active site in the variant S/R pairs. In this regard, future studies investigating the dynamic behavior of these KLIs would provide valuable insights into how these KLIs can be further engineered to more efficiently assist formation of the active site in the VS ribozyme.

CONCLUDING REMARK

Despite the ability of the VS ribozyme to specifically cleave a stem-loop substrate, very few studies had previously explored the possibility of modifying the VS ribozyme for cleavage of alternate substrates. Using a novel RNA engineering approach, we demonstrated here that the KLI within the VS ribozyme could be substituted by at least two other known KLIs while maintaining substantial cleavage activity. Interestingly, the possibility of substituting the KLI broadens the substrate specificity of VS ribozyme derivatives, which can now target SLI variants in which the 7-nt terminal loop can be replaced by at least three other 6-nt loop sequences and the length of the adjoining stem can be varied to some extent. Future engineering efforts are now geared toward improving the cleavage efficiency of the VS ribozyme variants identified here as well as further broadening the substrate specificity of VS ribozyme derivatives.

SUPPLEMENTARY DATA

Supplementary Data are available at NAR Online.

ACKNOWLEDGEMENTS

The authors thank Dominique Chaussé for RNA preparation, Ryan Richter for computer support, as well as James G. Omichinski for discussions and critical reading of the manuscript. They also thank Sébastien Lemieux and Calcul Québec for providing computing facilities.

FUNDING

Canadian Institutes of Health Research [CIHR MOP-86502 to P.L.]; CIHR and Université de Montréal Ph.D. Scholarships (to J.L.-L.); FRQNT Ph.D. Scholarship (to P.D.). Funding for open access charge: CIHR.
Conflict of interest statement. None declared.

REFERENCES

1. Lilley,D.M. (2011) Catalysis by the nucleolytic ribozymes. *Biochem. Soc. Trans.*, **39**, 641–646.
2. Jimenez,R.M., Polanco,J.A. and Luptak,A. (2015) Chemistry and biology of self-cleaving ribozymes. *Trends Biochem. Sci.*, **40**, 648–661.
3. Weinberg,Z., Kim,P.B., Chen,T.H., Li,S., Harris,K.A., Lunse,C.E. and Breaker,R.R. (2015) New classes of self-cleaving ribozymes revealed by comparative genomics analysis. *Nat. Chem. Biol.*, **11**, 606–610.
4. Harris,K.A., Lunse,C.E., Li,S., Brewer,K.I. and Breaker,R.R. (2015) Biochemical analysis of pistol self-cleaving ribozymes. *RNA*, **21**, 1852–1858.
5. Li,S., Lunse,C.E., Harris,K.A. and Breaker,R.R. (2015) Biochemical analysis of hatchet self-cleaving ribozymes. *RNA*, **21**, 1845–1851.
6. Herschlag,D. (2015) Learning from ribozymes. *RNA*, **21**, 527–528.
7. Collins,R.A. (2002) The *Neurospora* Varkud satellite ribozyme. *Biochem. Soc. Trans. Rev.*, **30**, 1122–1126.
8. Lilley,D.M. (2004) The Varkud satellite ribozyme. *RNA*, **10**, 151–158.
9. Wilson,T.J. and Lilley,D.M. (2013) A mechanistic comparison of the Varkud satellite and hairpin ribozymes. *Prog. Mol. Biol. Transl. Sci.*, **120**, 93–121.
10. Guo,H.C.T. and Collins,R.A. (1995) Efficient trans-cleavage of a stem-loop RNA substrate by a ribozyme derived from *Neurospora* VS RNA. *EMBO J.*, **14**, 368–376.
11. Rastogi,T., Beattie,T.L., Olive,J.E. and Collins,R.A. (1996) A long-range pseudoknot is required for activity of the *Neurospora* VS ribozyme. *EMBO J.*, **15**, 2820–2825.
12. Leontis,N.B. and Westhof,E. (2001) Geometric nomenclature and classification of RNA base pairs. *RNA*, **7**, 499–512.
13. Bouchard,P. and Legault,P. (2014) Structural insights into substrate recognition by the *Neurospora* Varkud satellite ribozyme: importance of U-turns at the kissing-loop junction. *Biochemistry*, **53**, 258–269.
14. Suslov,N.B., DasGupta,S., Huang,H., Fuller,J.R., Lilley,D.M., Rice,P.A. and Piccirilli,J.A. (2015) Crystal structure of the Varkud satellite ribozyme. *Nat. Chem. Biol.*, **11**, 840–846.
15. Andersen,A. and Collins,R.A. (2000) Rearrangement of a stable RNA secondary structure during VS ribozyme catalysis. *Mol. Cell*, **5**, 469–478.
16. Andersen,A.A. and Collins,R.A. (2001) Intramolecular secondary structure rearrangement by the kissing interaction of the *Neurospora* VS ribozyme. *Proc. Natl. Acad. Sci. U.S.A.*, **98**, 7730–7735.
17. Zamel,R. and Collins,R.A. (2002) Rearrangement of substrate secondary structure facilitates binding to the *Neurospora* VS ribozyme. *J. Mol. Biol.*, **324**, 903–915.
18. Bouchard,P. and Legault,P. (2014) A remarkably stable kissing-loop interaction defines substrate recognition by the *Neurospora* VS Ribozyme. *RNA*, **20**, 1451–1464.
19. Hiley,S.L. and Collins,R.A. (2001) Rapid formation of a solvent-inaccessible core in the *Neurospora* Varkud satellite ribozyme. *EMBO J.*, **20**, 5461–5469.
20. Jones,F.D. and Strobel,S.A. (2003) Ionization of a critical adenosine residue in the *Neurospora* Varkud satellite ribozyme active site. *Biochemistry*, **42**, 4265–4276.
21. McLeod,A.C. and Lilley,D.M. (2004) Efficient, pH-dependent RNA ligation by the VS ribozyme in trans. *Biochemistry*, **43**, 1118–1125.

22. Zhao,Z.Y., McLeod,A., Harusawa,S., Araki,L., Yamaguchi,M., Kurihara,T. and Lilley,D.M. (2005) Nucleobase participation in ribozyme catalysis. *J. Am. Chem. Soc.*, **127**, 5026–5027.
23. Smith,M.D. and Collins,R.A. (2007) Evidence for proton transfer in the rate-limiting step of a fast-cleaving Varkud satellite ribozyme. *Proc. Natl. Acad. Sci. U.S.A.*, **104**, 5818–5823.
24. Wilson,T.J., McLeod,A.C. and Lilley,D.M. (2007) A guanine nucleobase important for catalysis by the VS ribozyme. *EMBO J.*, **26**, 2489–2500.
25. Jaikaran,D., Smith,M.D., Mehdizadeh,R., Olive,J. and Collins,R.A. (2008) An important role of G638 in the cis-cleavage reaction of the *Neurospora* VS ribozyme revealed by a novel nucleotide analog incorporation method. *RNA*, **14**, 938–949.
26. Smith,M.D., Mehdizadeh,R., Olive,J.E. and Collins,R.A. (2008) The ionic environment determines ribozyme cleavage rate by modulation of nucleobase pKa. *RNA*, **14**, 1942–1949.
27. Wilson,T.J., Li,N.S., Lu,J., Frederiksen,J.K., Piccirilli,J.A. and Lilley,D.M. (2010) Nucleobase-mediated general acid-base catalysis in the Varkud satellite ribozyme. *Proc. Natl. Acad. Sci. U.S.A.*, **107**, 11751–11756.
28. Guo,H.C.T., De Abreu,D.M., Tillier,E.R.M., Saville,B.J., Olive,J.E. and Collins,R.A. (1993) Nucleotide sequence requirements for self-cleavage of *Neurospora* VS RNA. *J. Mol. Biol.*, **232**, 351–361.
29. Beattie,T.L., Olive,J.E. and Collins,R.A. (1995) A secondary-structure model for the self-cleaving region of *Neurospora* VS RNA. *Proc. Natl. Acad. Sci. U.S.A.*, **92**, 4686–4690.
30. Rastogi,T. and Collins,R.A. (1998) Smaller, faster ribozymes reveal the catalytic core of *Neurospora* VS RNA. *J. Mol. Biol.*, **277**, 215–224.
31. Bouchard,P., Lacroix-Labonté,J., Desjardins,G., Lampron,P., Lisi,V., Lemieux,S., Major,F. and Legault,P. (2008) Role of SLV in SLI substrate recognition by the *Neurospora* VS ribozyme. *RNA*, **14**, 736–748.
32. Lacroix-Labonté,J., Girard,N., Lemieux,S. and Legault,P. (2012) Helix-length compensation studies reveal the adaptability of the VS ribozyme architecture. *Nucleic Acids Res.*, **40**, 2284–2293.
33. Petrov,A.I., Zirbel,C.L. and Leontis,N.B. (2011) WebFR3D–a server for finding, aligning and analyzing recurrent RNA 3D motifs. *Nucleic Acids Res.*, **39**, W50–W55.
34. Merino,E.J., Wilkinson,K.A., Coughlan,J.L. and Weeks,K.M. (2005) RNA structure analysis at single nucleotide resolution by selective 2'-hydroxyl acylation and primer extension (SHAPE). *J. Am. Chem. Soc.*, **127**, 4223–4231.
35. Chang,K.Y. and Tinoco,I. Jr (1997) The structure of an RNA "kissing" hairpin complex of the HIV TAR hairpin loop and its complement. *J. Mol. Biol.*, **269**, 52–66.
36. Magee,T.V., Han,S., McCurdy,S.P., Nguyen,T.T., Granskog,K., Marr,E.S., Maguire,B.A., Huband,M.D., Chen,J.M., Subashi,T.A. *et al.* (2013) Novel 3-O-carbamoyl erythromycin A derivatives (carbamolides) with activity against resistant staphylococcal and streptococcal isolates. *Bioorg. Med. Chem. Lett.*, **23**, 1727–1731.
37. Major,F., Turcotte,M., Gautheret,D., Lapalme,G., Fillion,E. and Cedergren,R. (1991) The combination of symbolic and numerical computation for three-dimensional modeling of RNA. *Science*, **253**, 1255–1260.
38. Lavery,R., Moakher,M., Maddocks,J.H., Petkeviciute,D. and Zakrzewska,K. (2009) Conformational analysis of nucleic acids revisited: Curves+. *Nucleic Acids Res.*, **37**, 5917–5929.
39. Eisenthal,R., Danson,M.J. and Hough,D.W. (2007) Catalytic efficiency and k_{cat}/K_M: a useful comparator? *Trends Biotechnol.*, **25**, 247–249.
40. Campbell,D.O., Bouchard,P., Desjardins,G. and Legault,P. (2006) NMR structure of Varkud satellite ribozyme stem-loop V in the presence of magnesium ions and localization of metal-binding sites. *Biochemistry*, **45**, 10591–10605.
41. Desjardins,G., Bonneau,E., Girard,N., Boisbouvier,J. and Legault,P. (2011) NMR structure of the A730 loop of the *Neurospora* VS ribozyme: insights into the formation of the active site. *Nucleic Acids Res.*, **39**, 4427–4437.
42. Bonneau,E. and Legault,P. (2014) Nuclear magnetic resonance structure of the III-IV-V three-way junction from the Varkud satellite ribozyme and identification of magnesium-binding sites using paramagnetic relaxation enhancement. *Biochemistry*, **53**, 6264–6275.
43. Bonneau,E., Girard,N., Lemieux,S. and Legault,P. (2015) The NMR structure of the II-III-VI three-way junction from the *Neurospora* VS ribozyme reveals a critical tertiary interaction and provides new insights into the global ribozyme structure. *RNA*, **21**, 1621–1632.
44. Wilkinson,K.A., Vasa,S.M., Deigan,K.E., Mortimer,S.A., Giddings,M.C. and Weeks,K.M. (2009) Influence of nucleotide identity on ribose 2'-hydroxyl reactivity in RNA. *RNA*, **15**, 1314–1321.
45. McGinnis,J.L., Dunkle,J.A., Cate,J.H. and Weeks,K.M. (2012) The mechanisms of RNA SHAPE chemistry. *J. Am. Chem. Soc.*, **134**, 6617–6624.